

This article was published as

Materials Science & Engineering C 118 (2021) 111476

DOI: <https://doi.org/10.1016/j.msec.2020.111476>

1 ***In vivo* time-course biocompatibility assessment of biomagnetic nanoparticles-based biomaterials for tissue**  
2 **engineering applications**

3  
4 Fernando Campos<sup>1,5</sup>, Ana Belén Bonhome-Espinosa<sup>3</sup>, Ramón Carmona<sup>4</sup>, Juan de Dios García López-Durán<sup>3,5</sup>,  
5 Pavel Kuzhir<sup>6</sup>, Miguel Alaminos<sup>1,5</sup>, Modesto Torcuato López-López<sup>3,5\*</sup>, Ismael Angel Rodriguez<sup>1,2,a\*</sup>, Víctor  
6 Carriel<sup>1,5,a</sup>

7  
8 <sup>1</sup>-Department of Histology, Tissue Engineering Group, Faculty of Medicine, University of Granada, Granada,  
9 Spain.

10 <sup>2</sup>-Department of Histology, Faculty of Dentistry, Nacional University of Cordoba, Cordoba, Argentina.

11 <sup>3</sup>-Department of Applied Physics, University of Granada, Avenida de la Fuente Nueva, 18071 Granada, Spain.

12 <sup>4</sup>-Department of Cell Biology, Faculty of Sciences, University of Granada, Campus Fuentenueva s/n, Granada,  
13 Spain.

14 <sup>5</sup>-Instituto de Investigación Biosanitaria ibs.GRANADA, Granada, Spain.

15 <sup>6</sup>-Laboratory of Physics, Matière Condensée, CNRS UMR 6622, University of Nice, Parc Valrose, 06108, Nice,  
16 Cedex2, France.

17 <sup>a</sup> These authors contributed equally: Víctor Carriel, Ismael Angel Rodriguez.

18  
19 \* Corresponding: Prof. Dr. Modesto Torcuato López-López & Prof. Dr. Ismael Rodriguez, Department of Applied  
20 Physics and Department of Histology, Tissue Engineering Group, University of Granada, Granada, Spain. Email:  
21 [modesto@ugr.es](mailto:modesto@ugr.es); [ismael.rodriguez@unc.edu.ar](mailto:ismael.rodriguez@unc.edu.ar)

22  
23  
24 **Abstract:**

25 Novel artificial tissues with potential usefulness in local-based therapies have been generated by tissue engineering  
26 using magnetic-responsive nanoparticles (MNPs). In this study, we performed a comprehensive *in vivo*  
27 characterization of bioengineered magnetic fibrin-agarose tissue-like biomaterials. First, *in vitro* analyses were  
28 performed and the cytocompatibility of MNPs was demonstrated. Then, bioartificial tissues were generated and  
29 subcutaneously implanted in Wistar rats and their biodistribution, biocompatibility and functionality were analysed  
30 at the morphological, histological, haematological and biochemical levels as compared to injected MNPs.  
31 Magnetic Resonance Image (MRI), histology and magnetometry confirmed the presence of MNPs restricted to the  
32 grafting area after 12 weeks. Histologically, we found a local initial inflammatory response that decreased with  
33 time. Structural, ultrastructural, haematological and biochemical analyses of vital organs showed absence of  
34 damage or failure. This study demonstrated that the novel magnetic tissue-like biomaterials with improved  
35 biomechanical properties fulfil the biosafety and biocompatibility requirements for future clinical use and support  
36 the use of these biomaterials as an alternative delivery route for magnetic nanoparticles.

37  
38 **Key words:** Tissue Engineering, Magnetic nanoparticles, Biomaterials, Bio-distribution, *In vivo* biocompatibility

## 42 1. Introduction

43 During the last years, magnetic nanoparticles (MNPs) have been evaluated in biomedicine for hyperthermia  
44 induction [1], cell labelling and separation [2], DNA separation [3], magnetic resonance imaging [4] and for drug  
45 or gene therapies [5, 6]. Iron oxide MNPs are the most commonly used, especially  $\text{Fe}_3\text{O}_4$  (magnetite) and  $\gamma\text{-Fe}_2\text{O}_3$   
46 (maghemite), because these are stable from a thermal, chemical and colloidal standpoint. In addition, based on the  
47 MNPs magnetic properties, it was hypothesized that these particles could be guided to specific *in vivo* locations  
48 using a magnetic field gradient. This could be useful as an alternative method to concentrate growth factors, drugs  
49 or cells associated to the particles [7-9], and it has been postulated that MNPs could be useful tools for theranostic  
50 [10] and local-based tissue engineering applications [11-15]. MNPs were previously tested for the generation of  
51 bioengineered magnetic tissue-like substitutes with improved properties without affecting cell adhesion,  
52 proliferation, viability or differentiation *in vitro* [16, 17], showing a significant improvement of the biomechanical  
53 properties of these biomaterials [13, 17].

54 Concerning the *in vivo* biodistribution of MNPs, it is clear that the administration route is a critical factor  
55 determining bioavailability and *in vivo* functionality of MNPs [10]. To the date, several studies focused on  
56 determining the fate of these particles when injected into the bloodstream [10] and results demonstrated that  
57 injected MNPs have a short lifespan, tend to accumulate in different organs and may have a certain degree of  
58 cytotoxic effects [10, 18]. However, the *in vivo* biodistribution of particles used within biomaterials needs further  
59 characterization [14], and *in vivo* studies evaluating the cellular and molecular processes related to biocompatibility,  
60 biodegradability and biodistribution of implanted magnetic hydrogels are in need. Our group previously developed  
61 a fibrin-agarose hydrogel (FAH), which was successfully used in numerous tissue engineering applications [19-  
62 26] and is currently used in clinical trials with the approval of the Spanish Agency of Medicines and Medical  
63 Devices (AEMPS) according to the EU guidelines for clinical use [27]. Therefore, FAH can be a useful carrier  
64 candidate to be combined with MNPs in order to generate novel biocompatible magnetic tissue-like biomaterials  
65 [12, 13, 17].

66 The aim of this study is to determine the biocompatibility of FAH-based magnetic tissue-like biomaterials  
67 containing MagNP-OH magnetic nanoparticles and to study their *in vivo* biodistribution in a rat model. First, the  
68 structure and biocompatibility of the magnetic hydrogels were determined *in vitro*. Then, magnetic scaffolds and  
69 scaffold-free MNPs were subcutaneously grafted in animals and the host response was evaluated by magnetic  
70 resonance imaging, laboratory testing, histology and magnetometry after 12 weeks *in vivo*.

71

## 72 2. Materials and methods

### 73 2.1 *In vitro* analyses

#### 74 2.1.1 Magnetic nanoparticles (MNPs) characterization

75 In this study, we used commercially available MNPs (Nanomyp, Granada, Spain) referred to as MagNP-OH. These  
76 MNPs are composed by a polycrystalline magnetite core coated with methyl methacrylate-co-hydroxyl ethyl  
77 methacrylate-co-ethylene glycol dimethacrylate (MMA-co-HEMA-co-EGDMA). The MagNP-OH particles were  
78 prepared for analyses following previously described procedures [13, 17].

79 The ultrastructure and dimensions of the MagNP-OH were determined by using a LIBRA 120 PLUS Carl Zeiss  
80 (Carl Zeiss, Oberkochen, Germany) transmission electron microscope (TEM). The magnetic properties of the  
81 MagNP-OH were characterized by a vibrating sample magnetometer VSM 4500 (EG&G Princeton Applied  
82 Research, NJ).

## 83 **2.1.2 Analysis of biocompatibility of the MagNP-OH on 2D cell cultures**

### 84 **2.1.2.1 Cell culture and cell-MagNP-OH interaction model**

85 Human fibroblast, primary cultures obtained from human oral mucosa biopsies were cultured for 24 h in 24-well  
86 plates ( $2 \times 10^4$  cells/well) with Dulbecco's Modified Eagle Medium (DMEM) with 10 % Fetal Bovine Serum (FBS)  
87 and antibiotics/antimycotics commercial cocktail solution (all cell culture reagents from Sigma-Aldrich, Steinheim,  
88 Germany) at 37°C with 5% of CO<sub>2</sub>. MagNP-OH particles were added to cultured cells at a concentration of 0.5%  
89 and 1% (w/v) in DMEM (without FBS and antibiotics) and were kept in culture for 24 h, and biocompatibility was  
90 determined after this time. As positive controls of live cells (100% cell viability), the same cells were cultured  
91 without MagNP-OH particles. As negative controls (100% cytotoxicity), cells were incubated in the same medium  
92 with 1% of triton X-100 (PanReac AppliChem, Barcelona, Spain). Biocompatibility was analysed in six  
93 independent samples and viability was evaluated 4 times in each sample (24 measures per test and condition).

94

### 95 **2.1.2.2 In vitro assessment of MagNP-OH cytocompatibility**

96 Cytocompatibility was evaluated using a combination of morphological analyses, functional WST-1 cell  
97 viability/proliferation assay and quantification of free DNA released from dead cells (able to detect cell membrane  
98 structural integrity), as previously described [20, 28, 29]. First, the morphological changes associated with the  
99 presence of MagNP-OH were determined by phase contrast microscopy. Then, we analysed the metabolic activity  
100 of the human cells using commercially available WST-1 assays (Roche Diagnostic, Mannheim, Germany) using a  
101 Microplate Reader (Biochrom® Asys UVM340, Cambridge, UK) at a wavelength of 450–690 nm [20, 28]. Finally,  
102 the DNA-released as a consequence of irreversible cell membrane damage was quantified by using a NanoDrop  
103 2000 UV-vis spectrophotometer (Thermo Fisher Scientific, Waltham, MA, USA) [14, 20].

104

### 105 **2.1.2.3 Preparation of the magnetic tissue-like biomaterials**

106 In this study, we prepared three types of scaffolds: non-magnetic FAH, and two types of magnetic FAH: FAH  
107 containing MagNP-OH (FAH-MNPs), and FAH containing MagNP-OH with the application of a definite magnetic  
108 field during gelation (FAH-MNPs-F). For the preparation of FAH and the magnetic scaffolds (FAH-MNPs and  
109 FAH-MNPs-F), we used a variation of a previously described method for non-magnetic FAH [19, 20, 22, 29, 30].  
110 Briefly, hydrogels were generated by mixing 70% of human plasma, 13.5% of PBS (0.1M, pH 7.2-7.4) containing  
111 or not MagNP-OH (0.5% v/v of final hydrogel volume) and 1.5% of tranexamic acid (Amchafibrin, Fides-  
112 Ecofarma, Valencia, Spain). This solution was carefully mixed and then, a 2% solution of CaCl<sub>2</sub> was added (10%  
113 of the final volume) to promote fibrin gelation, followed by 5% volume of melted 2% type VII agarose (both by  
114 Sigma-Aldrich, Steinheim, Germany) in PBS. This mixture was aliquoted and kept in a cell incubator using  
115 standard culture conditions until complete gelation [13]. In the case of FAH-MNPs-F, the mixture was subjected  
116 to a vertical magnetic field (48 kA/m) during the first 5 minutes of the process of jellification to obtain an  
117 anisotropic biomaterial composed by aligned fibres as previously reported [13]. The process, by which the  
118 hydrogel is formed, has been previously described [20, 22, 28]. Concisely, an addition of CaCl<sub>2</sub> can activate the  
119 blood coagulation factors of the human plasma, resulting in the cleavage of fibrinogen by thrombin, with the  
120 subsequent polymerization of fibrin monomers into an insoluble fibrin gel [31]. At the same time, the agarose  
121 polysaccharides jellify by forming hydrogen bonds on the fibrin fibres as temperature decreases [32, 33].

122

123

#### 124 **2.1.2.4 Analysis of biomechanical properties of the magnetic tissue-like biomaterials**

125 Magnetic and non-magnetic tissue-like biomaterials were subjected to oscillatory shear strains of increasing  
126 amplitude and fixed frequency (1 Hz), and the corresponding oscillatory shear stress was assessed using a Haake  
127 MARS III (Thermo Fisher Scientific, Waltham, MA, USA) rheometer at 37°C. The measuring system geometry  
128 was a 3.5 cm diameter parallel plate set with rough surfaces to avoid wall slip, and the rotating plate was adjusted  
129 to a normal force of 5 N. Measurements were conducted under oscillatory shear strains and the biomechanical  
130 properties of the different tissue-like biomaterials were studied by determining the complex viscoelastic modulus  
131 of each sample.

132

### 133 **2.2 In vivo analyses**

#### 134 **2.2.1 Laboratory animals**

135 In this study, a total of eighty-five 12-week-old adult male Wistar rats weighing 250–300 g were used. Animals  
136 were maintained in the Experimental Unit of the University Hospital Virgen de las Nieves in Granada (Spain).  
137 Animals were housed in a temperature-controlled room ( $21 \pm 1^\circ\text{C}$ ) on a 12 h light/dark cycle with *ad libitum* access  
138 to tap water and standard rat chow. These studies were performed according to the European Union and Spanish  
139 Government guidelines for the ethical care of animals (EU Directive No. 63/2010, RD 53/2013) and this project  
140 was approved by the CEEA ethical committee for animal experimentation (approval number: 03-7-15-311).

141

#### 142 **2.2.2 Surgical procedure and experimental groups**

143 For the *in vivo* biocompatibility evaluation of magnetic tissue-like biomaterials, and to study the biodistribution of  
144 the MagNP-OH, animals were deeply anaesthetized by intraperitoneal injection of a mixture of acepromazine  
145 (Calmo-Neosan®, 0.001 mg/g of the weight of the animal, Boehringer Ingelheim, Ingelheim am Rhein, Germany)  
146 and ketamine (Imalgene 1000®, 0.15 mg/g of the weight of the animal, Boehringer Ingelheim). Each animal was  
147 randomly assigned to one of the following experimental groups ( $n = 20$  in each except for the control group):

148 - (i) FAH group: once anaesthetized, a 1 cm-long incision was made in the forearm skin of each animal, a  
149 FAH tissue-like substitute was subcutaneously grafted, and the injury was repaired using absorbable sutures. These  
150 animals were used as a control group.

151 - (ii) FAH-MNPs group: in these animals, FAH containing 0.5% (v/v) MagNP-OH were implanted  
152 following the same procedure described for the FAH group.

153 - (iii) FAH-MNPs-F group: FAH containing 0.5% (v/v) MagNP-OH subjected to a magnetic field during  
154 gelation were implanted.

155 - (iv) MNPs-INJ group: in this case, MNPs were injected in the same area of groups i, ii and iii (forearm  
156 subcutaneous tissue). In this sense, subcutaneous injection of a solution containing the MNPs was given in both  
157 forearms of each rat (250  $\mu\text{l}$  of a sterile physiological solution containing 12.5 mg of MagNP-OH).

158 - (v) CTR group: five healthy animals were used as controls.

159 Animals were euthanized after 1, 3, 5 or 12 weeks ( $n = 5$  in each period) by using an overdose of anaesthetics  
160 followed by intracardiac perfusion of fixative.

161

#### 162 **2.2.3 Magnetic resonance imaging (MRI)**

163 Magnetic Resonance Image (MRI) analysis was used to identify the grafted materials in each animal and to assess  
164 the effects of these materials on the morphology of some major body organs. For this purpose, 3 animals

165 corresponding to each experimental group (CTR, FAH, FAH-MNPs, FAH-MNPs-F and MNPs-INJ) were  
166 analysed after 1, 3, 5, and 12 weeks of the surgical procedure using a Biospec TM 70/20 USR device equipped  
167 with 7 Tesla Ultrashield Refrigerated magnets (Bruker, Billerica, MA). This device was designed and optimized  
168 for the analysis of small experimentation animals and is available at the Scientific Research Facility of the  
169 University of Granada, Spain. First, animals were anesthetized with isoflurane using a Ohmeda veterinary  
170 anaesthesia unit and immobilized in a MRI-compatible cradle. Temperature was kept at 37°C using a water bath  
171 circulation system. Then, a whole-body scan was performed on each animal, and the morphology of liver, kidneys,  
172 lymph nodes and spleen was evaluated, and the grafting site was specifically analysed to determine the MRI  
173 morphology of the implant site and possible migration of the particles to local and regional tissues. In all cases,  
174 high resolution axial T2-weighted images were acquired through a T2-TurboRARE sequence using the following  
175 settings and experimental conditions: echo time = 23 ms; rare factor = 8 and slice thickness = 1 mm; repetition  
176 time = 1371.177 ms with average = 8.

177

#### 178 **2.2.4 Haematological and biochemical studies**

179 1.5 mL of blood was collected from 5 animals corresponding to each experimental condition at 1, 3, 5 and 12  
180 weeks of *in vivo* follow-up. Blood was stored in Eppendorf tubes containing 5% heparin. For complete blood  
181 count, a Sysmex KX-21N automatic analyser (Roche Laboratories, Basel, Switzerland) was used as previously  
182 described [32] to determine the following haematological parameters: concentration of haemoglobin (HGB),  
183 erythrocytes count (RCB), haematocrit count (HCT), platelets (PLT), white blood cells (WBC), lymphocytes  
184 (LYM), neutrophils (NEUT), monocytes-basophils-eosinophils (MXD) [34, 35].

185 For biochemical tests, blood was centrifuged for 15 min at 3,500 rpm and the supernatant serum was collected for  
186 analysis using a clinical chemistry analyser Cobas c311 (Roche Laboratories, Basel, Switzerland). The following  
187 biochemical parameters were analysed in each sample: Alanine aminotransferase (ALT), urea (UREA), creatinine  
188 (CREJ2), iron (IRON2) (all RTU kits from Roche Laboratories) [34, 35].

189

#### 190 **2.2.5 Histological and histochemical studies**

191 For the histological analyses, animals were deeply anaesthetized and perfused with 4% neutral buffered  
192 paraformaldehyde. For all animals included in the study, the area of the implant (FAH, FAH-MNPs, FAH-MNPs-  
193 F and MNPs-INJ) was carefully dissected and post-fixed in 4% neutral buffered formaldehyde for 24 h, dehydrated  
194 and embedded in paraffin. For animals corresponding to 1 and 12 weeks of follow-up, four vital organs (liver,  
195 kidneys, lymph nodes and spleen) were also extracted, post-fixed and embedded in paraffin. Tissue blocks were  
196 sectioned at 5 µm of thickness, rehydrated and stained with haematoxylin-eosin (H&E) for histological evaluation.  
197 In addition, different histochemical techniques were used to determine tissue-specific normal parameters. The  
198 periodic acid-Schiff histochemical method (PAS) was used to evaluate the glycogen content of the liver, the  
199 glomerular basement membrane of the kidney and the basement membranes of each tissue and organ. To identify  
200 the presence of ferric iron, all tissues and organs were stained with Perls (Prussian blue reaction) histochemical  
201 method contrasted with H&E as described previously [14].

202 The percentage of positive area for Perls-positive histochemical reaction in the spleen was determined with ImageJ  
203 software (National Institutes of Health, USA) from each group at 1 and 12 weeks following a previously described  
204 methodology [28, 36].

205

## 206 2.2.6 Ultrastructural analyses

207 For the ultrastructural analyses, tissue samples corresponding to the 12 weeks follow-up period were obtained  
208 from each animal included in the *in vivo* study at the moment of the euthanasia. Samples were fixed in 2.5%  
209 glutaraldehyde, washed three times in cacodylate buffer and post-fixed in 1% osmium tetroxide. Tissues were then  
210 dehydrated and embedded in epoxy resin, and sectioned. Ultrathin sections were stained with aqueous uranyl  
211 acetate and lead citrate, mounted on grids and analysed in a Carl Zeiss EM902 transmission electron microscope.  
212 The presence of iron atoms in tissues was identified by Electron Energy-Loss Spectroscopy (EELS). Analysis of  
213 the heterogeneous pattern of the FAH, FAH-MNPs and FAH-MNPs-F was carried out by scanning electron  
214 microscopy (SEM) using a FEI Quanta 200 equipment (Hillsboro, OR) as previously described [20, 22, 28].

215

## 216 2.2.7 Magnetometry

217 After the euthanasia, we tracked the presence of particles at the site of implantation and vital organs. We checked  
218 the magnetic response of the samples with a neodymium magnet in a magnetic field gradient of 10 mT/mm and a  
219 maximum field of 470 mT. In addition, we quantified the magnetic response of the samples through magnetometry  
220 measurements using a vibrating sample magnetometer VSM 4500 (EG&G Princeton Applied Research, NJ) at  
221 room temperature. For this, similar volumes of tissue (equivalent to 50 mg of mass) were used from each condition.  
222 The detection limit of the magnetometer was 0.001 emu/g, which corresponds to approximately 30  $\mu\text{g}$  of particles.  
223 These analyses were performed in animals corresponding to 12 weeks of *in vivo* follow-up.

224

## 225 2.2.8 Statistical analyses

226 In this study, all variables were subjected to the Shapiro-Wilk test of normality and resulted to be non-normally  
227 distributed. Therefore, Fisher Exact Test and Mann-Whitney *U* test were used to determine statistical differences  
228 between comparison groups. All variables were analysed by using the software SPSS 16.00 (IBM Company,  
229 Armonk, NY) and results were shown as mean  $\pm$  standard deviation (SD). In this study,  $p < 0.05$  was considered  
230 as statistically significant in two-tailed tests.

231

## 232 3. Results and Discussion

### 233 3.1 *In vitro* characterization and biocompatibility

234 First, our ultrastructural analysis of the MagNP-OH used in this study allowed us to confirm that the diameter of  
235 the particles was  $70 \pm 18$  nm, which is higher than MNPs frequently used by other authors in tissue engineering  
236 applications (30-40 nm) [15, 16, 37-41]. Interestingly, particles tended to form polycrystalline aggregates  
237 externally coated by a polymeric matrix surrounding each aggregate (Figure 1A). Magnetic characterization of the  
238 MagNP-OH revealed the typical soft ferromagnetic character of these MNPs, with negligible remnant  
239 magnetization, and a saturation magnetization of  $161 \pm 7$  kA/m (Figure 1B). It is well known that the size of the  
240 MNPs is directly related to the magnetic response of the particles, and multidomain MNPs ( $> 50$  nm) commonly  
241 show higher magnetic response as compared to small particles [38]. However, it has been previously demonstrated  
242 that biointegration of large MNPs in a hydrogel mesh tend to be incomplete due to gravitational settling and lower  
243 total surface area of these MNPs [14]. Although MNPs with a larger diameter will show stronger magnetic  
244 response [14], the present work was carried out with smaller nanoparticles in order to favour biointegration in the  
245 fibrin-agarose mesh. Further research is in need to determine the optimal size of the MNPs for use in the generation

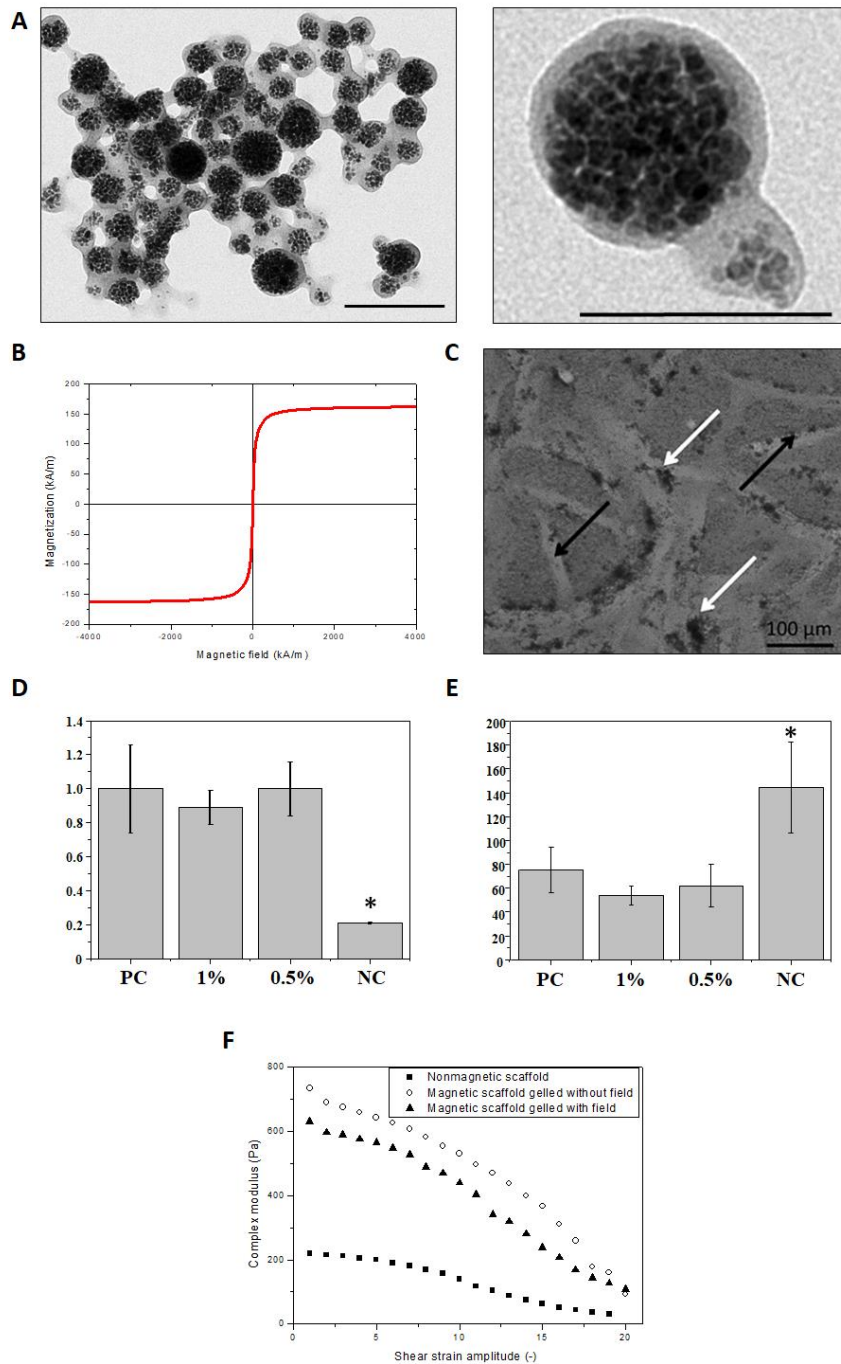
246 of magnetic hydrogels, and the possibility of using particles of different sizes in the same hydrogel. In fact, the *in*  
247  *vivo* biological effects of MNPs have been demonstrated to be size-dependent [42].  
248 Regarding *in vitro* cytocompatibility of human cells cultured in the presence of MagNP-OH, we carried out a  
249 multi-level approach analysis at three levels: cell morphology, cell function and integrity of the cell membrane.  
250 Results show that, in general, MNPs are highly cytocompatible. In the first place, co-culture of these MNPs with  
251 human cells was not able to modify the typical elongated spindle-like shape of viable human fibroblasts, suggesting  
252 that these cells remained highly viable, and MNPs were mostly found homogeneously distributed in the  
253 extracellular space of the cells (Fig. 1C). In fact, the morphology of these cells was comparable to positive control  
254 cells cultured without MNPs and very different from the small, rounded-shape appearance of negative control dead  
255 cells. To confirm these results at the functional level, we then analysed the functionality of the cellular  
256 mitochondrial dehydrogenase by WST-1 assay. Results showed high levels of metabolic activity in cells containing  
257 MagNP-OH (at the concentration of 1% and 0.5%) with values comparable ( $p > 0.05$ ) to the positive control group.  
258 Positive controls and both experimental groups containing MagNP-OH showed significantly higher WST-1 values  
259 as compared to the negative control group ( $p < 0.0001$ ) (Figure 1D), suggesting high metabolic activity [20, 28].  
260 Finally, viability was analysed at the structural level by quantifying released DNA from cells cultivated in the  
261 presence of the MagNP-OH (Figure 1E), which is unfailingly associated to a cell membrane disruption [20, 28].  
262 Results showed low cell mortality in positive controls and both experimental groups (1% and 0.5%), with no  
263 differences between positive controls and cells cultured with MagNP-OH ( $p > 0.05$ ). However, mortality was  
264 significantly higher in negative controls ( $p = 0.0020$ ). These results are in agreement with the high  
265 cytocompatibility previously observed in hydrogels containing MagNP-OH [17], especially when these particles  
266 were coated with a polymer such as polyethylene glycol (PEG) [14]. The polymeric coating of MNPs provides  
267 hydrophilic properties that may improve stabilization in colloidal suspension and increase biocompatibility [10,  
268 43]. Altogether, these results support the high *in vitro* biocompatibility of the coated MagNP-OH used in this  
269 study.

270 Once the cytocompatibility of MagNP-OH was evaluated *in vitro*, we generated magnetic tissue-like biomaterials  
271 containing these particles. The rheological characterization of FAH-MNPs and FAH-MNPs-F revealed that  
272 incorporation of MagNP-OH considerably increased the strength of the tissue-like biomaterials as compared to  
273 control nonmagnetic FAH for the complex viscoelastic modulus  $G^* = \left[ (G')^2 + (G'')^2 \right]^{1/2}$  (Figure 1F), for both  
274 the biomaterials subjected to magnetic fields during the polymerization and materials devoid of these fields. In  
275 agreement with our previous studies [20, 28, 36], SEM images confirmed that the use of a magnetic field induced  
276 the alignment of the MNPs within the fibrin-agarose network (Figure 2). These findings are in agreement with  
277 previous reports showing that MNPs can considerably improve the biomechanical properties of FAH, thus  
278 increasing their putative usefulness in tissue engineering and regenerative medicine [13, 14, 17]. Previous studies  
279 suggest that the biomechanical improvement observed by the incorporation of MNPs within FAH can be explained  
280 by two reasons: on the one hand, the strong electrostatic interactions established between the biomaterial network  
281 and the MNPs, and on the other hand, the formation of MNPs clusters within the biomaterials network [17]. The  
282 electrostatic interactions increase the overall molecular interaction forces of the resulting biomaterial network,  
283 therefore explaining the biomechanical improvement. Furthermore, it was demonstrated that the MNPs clusters  
284 act as knots, sites from where the fibrin network is organized in more compact, thicker and aligned fibrin strands



285 which create a biomechanically and structurally more efficient network as compared to the classical nonmagnetic  
286 hydrogels [17].

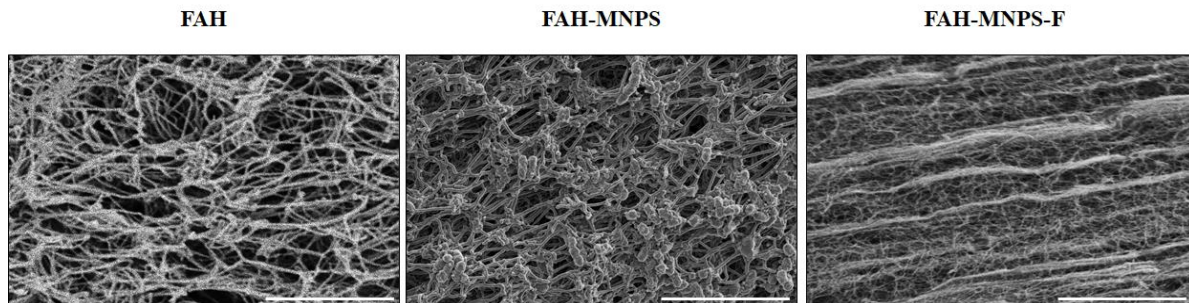
287  
288  
289



290 **Figure 1. *In vitro* characterization of the MagNP-OH particles used in this study.** A) Transmission electron  
291 microscopy ultrastructural analysis of MagNP-OH particles. Scale bar: 200 nm (left) and 100 nm (right). B)  
292 Magnetization curve of MagNP-OH particles. C) Phase contrast microscopy image of human fibroblasts cultured  
293 with MagNP-OH particles. Cells are labelled with black arrows and MagNP-OH particles are highlighted with  
294 white arrows. D) Results of the cellular metabolic activity as determined by WST-1 assay. E) Analysis of cell  
295 membrane integrity as determined by DNA quantification. In D and E, values correspond to averages and standard

296 deviations.\* Results are statistically different from all the other study groups. PC: positive controls; NC: negative  
297 controls. F) Biomechanical properties are shown as the complex viscoelastic modulus of nonmagnetic FAH, FAH-  
298 MNPs and FAH-MNPs-F.

299  
300  
301



302 **Figure 2. Representative images corresponding to the SEM analysis of materials used in this study.** FAH:  
303 fibrin-agarose hydrogels; FAH-MNPs: FAH containing MagNP-OH; FAH-MNPs-F: FAH containing MagNP-OH  
304 subjected to a magnetic field during gelation. Scale bar 10  $\mu$ m

305

### 306 **3.2 *In vivo* evaluation**

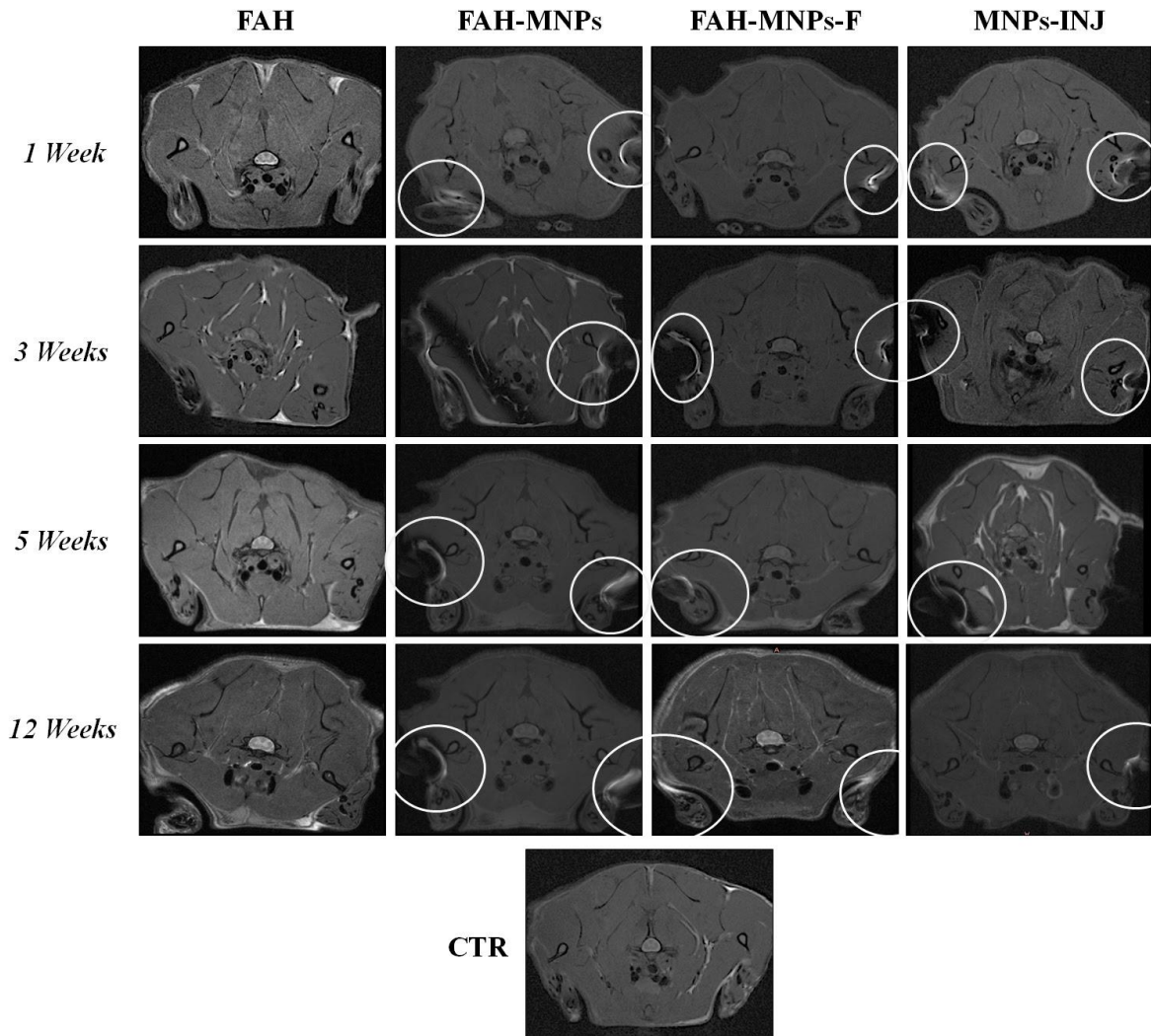
307 Accurate monitoring and analysis of the fate of MNPs grafted *in vivo* in laboratory animals is essential for their  
308 future clinical translation and practical application [44]. Ideally, the biocompatibility of grafted MNPs should be  
309 assessed by using a combination of invasive and non-invasive methods allowing a precise evaluation of the fate  
310 of the MNPs and the potential metabolic pathways and organs involved in MNPs metabolism and biodegradation.  
311 Consequently, animals grafted with the different materials were subjected to an array of highly accurate evaluation  
312 methods that included MRI, magnetometry, haematological, biochemical and histological analyses to determine  
313 biocompatibility and the outcome of the grafted materials. In addition, analyses were performed at the local and  
314 the distal level as requested by most National Medicines Agencies for Advanced Therapies Medicinal Products  
315 [45]. In this sense, we first analysed the local graft site to determine *in situ* biosafety, temporal stability and  
316 migration to neighbour tissues. Then, we analysed four key distal organs to shed light on the possible distal effects  
317 of the grafted biomaterials, including distal organ migration. In general, all these analyses allowed us to  
318 demonstrate that the biomaterials used in the present work were safe and complied with the main biosafety  
319 requirements for future clinical use.

320 *In situ* time-course analysis of the implant site using MRI (Fig. 3) showed that non-magnetic FAH remained at the  
321 grafting site and was locally metabolized and reabsorbed in 12 weeks. In contrast, magnetic biomaterials  
322 containing MagNP-OH, as well as the injected MagNP-OH remained located in the implant site after 12 weeks of  
323 *in vivo* follow-up (Fig. 3). These results coincide with the magnetometric analyses showing that controls and  
324 animals grafted with FAH were negative, whereas all animals with grafted MagNP-OH showed a highly positive  
325 magnetic response at the grafting site after 12 weeks of follow-up. Furthermore, the MRI analysis of distal organs  
326 did not reveal any sign of damage, inflammation or organ failure in any of the experimental groups during the  
327 whole follow-up period (Supplementary Fig. S1).

328

329

**MRI AT THE IMPLANTATION SITE**



332 **Figure 3. Magnetic Resonance Images (MRI) analysis of animals with the different materials grafted at each**  
 333 **study time.** Images were taken at the grafting site. White circles correspond to hyperintense areas corresponding  
 334 to MagNP-OH accumulation at the implantation site. CTR: control animals; FAH: fibrin-agarose hydrogels; FAH-  
 335 MNPs: FAH containing MagNP-OH; FAH-MNPs-F: FAH containing MagNP-OH subjected to a magnetic field  
 336 during gelation; MNPs-INJ: MNPs injected subcutaneously.

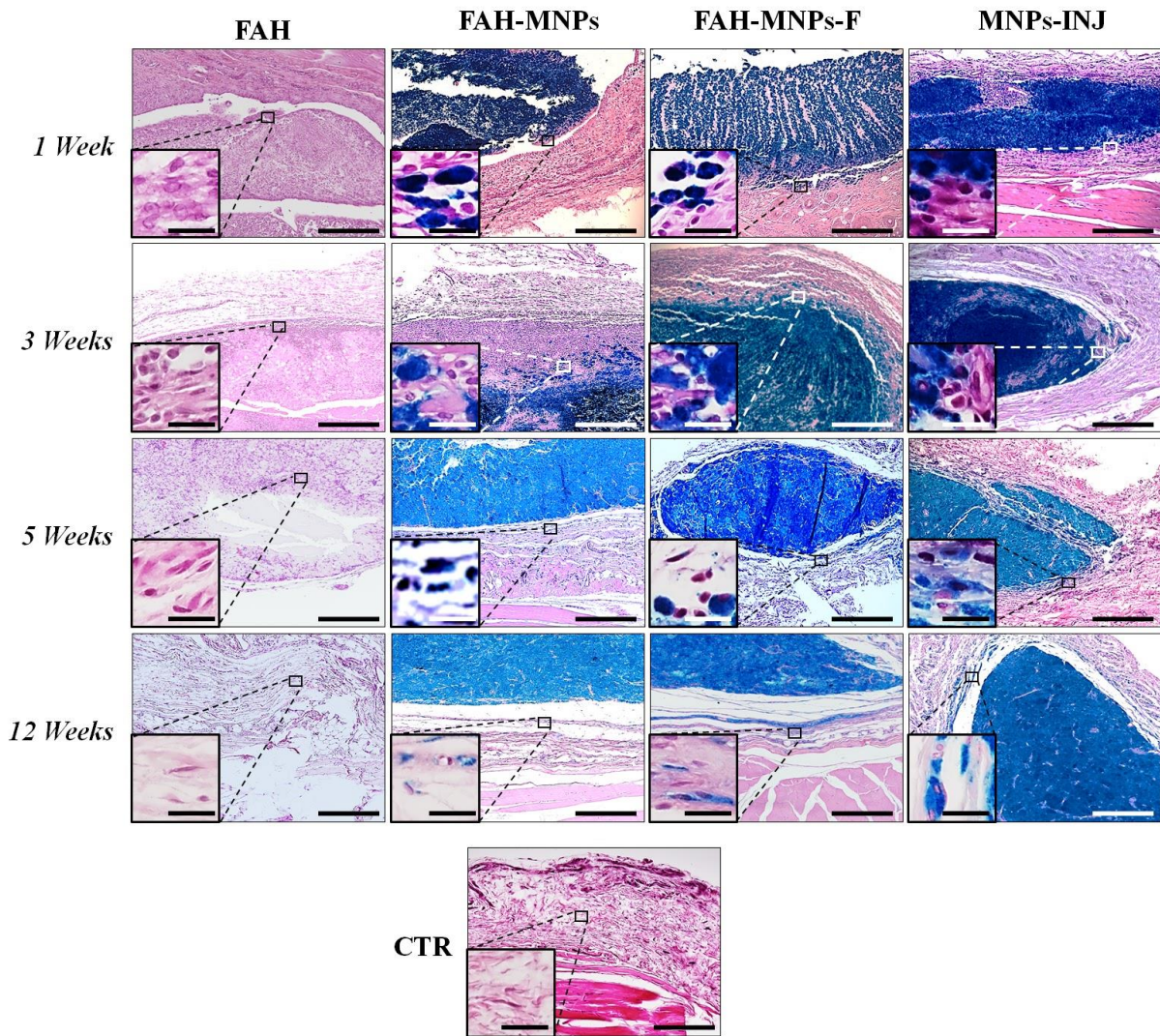
337  
 338 Then, the implantation site was analysed histologically. In this regard, most animals showed an initial mild local  
 339 inflammatory reaction restricted to the tissues surrounding the implanted materials, but no signs of necrosis,  
 340 infection, rejection or malignant transformation were found in any of the groups (Fig. 4). This reaction was similar  
 341 in all groups grafted with biomaterials (FAH, FAH-MNPs and FAH-MNPs-F), and tended to decrease over time.  
 342 In the FAH group, we found that the number of inflammatory cells, especially macrophages, decreased with time  
 343 and almost disappeared after 12 weeks. An interesting finding of our study was that the three groups in which  
 344 MNPs were grafted tended to encapsulate the grafts, with the formation of a central Perls-positive nucleus  
 345 surrounded by a connective tissue capsule. Although we found a single nucleus in the FAH-MNPs and FAH-  
 346 MNPs-F groups, particles tended to form several independent nuclei in the MNPs-INJ group, at least during the

347 first 5 weeks (Fig. 4). These results confirm the absence of an increased inflammatory reaction driven by the MNPs  
348 implant and point out the usefulness of the FAH-MNPs model as a straightforward way of providing the host tissue  
349 with MNPs that could exert a positive clinical effect [46, 47]. As compared to injection, surgical implantation of  
350 a tissue-like magnetic material allowed a more efficient control of the grafting site and, according to our results,  
351 favoured the MNPs containment and enhanced encapsulation of the whole grafted mass in a single nucleus, thus  
352 preventing the connective tissue infiltration and grafts disaggregation or dispersion found in the MNPs-INJ group.  
353 In addition, the MNPs corresponding to the FAH-MNPs-F group showed a clear definite alignment and orientation  
354 of the MNPs during the first weeks, even though this orientation was lost after 5 weeks. Interestingly, the loss of  
355 this characteristic alignment pattern obtained by the use of a magnetic field coincided with the *in vivo*  
356 biodegradation process of the FAH [34]. In this regard, we recently demonstrated that FAH biomaterials are  
357 progressively remodelled and infiltrated by host immune cells, mainly macrophages, being completely degraded  
358 after 5 to 9 weeks of *in vivo* implantation [23, 34]. We may hypothesize that the progressive degradation and  
359 remodelling of the FAH network supporting the aligned particles resulted in a loss of structural cohesion of the  
360 aligned MNPs clusters with the consequent loss of its aligned structural pattern [23, 34].  
361 The three-dimensional orientation of biomaterials is one of the goals of current tissue engineering, since most  
362 human tissues are characterized by a nonlinear and anisotropic mechanical behaviour [48] due to the non-random  
363 distribution of its components, and this distribution is essential for its proper *in vivo* function. The use of FAH-

364 MNPs-F could contribute to obtaining MNPs-based bioartificial tissues with defined alignment with added value  
 365 for use in regenerative medicine [49], as shown in Fig. 2.

366

367



368

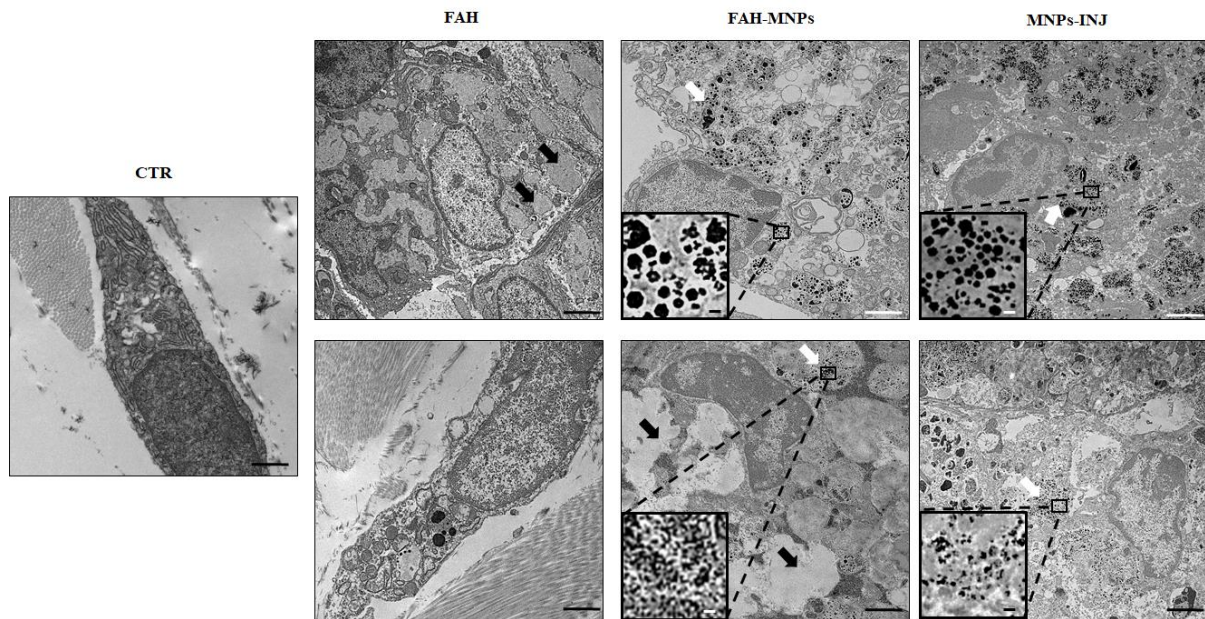
369 **Figure 4. Perl's histochemical results of grafted biomaterials and injected MNPs at 1, 3, 5 and 12 weeks *in***  
 370 ***vivo*.** CTR: control animals; FAH: fibrin-agarose hydrogels; FAH-MNPs: FAH containing MagNP-OH; FAH-  
 371 MNPs-F: FAH containing MagNP-OH subjected to a magnetic field during gelation; MNPs-INJ: MNPs injected  
 372 subcutaneously. The inserts images correspond to higher magnifications of the same images. Scale bars: 300  $\mu$ m  
 373 (large images) and 20  $\mu$ m (inserts).

374

375 Furthermore, we carried out TEM analyses to determine the biocompatibility of each biomaterial at the  
 376 ultrastructural level after 12 weeks of the surgical procedure. On the one hand, host tissues corresponding to the  
 377 FAH group showed some macrophages with intracellular phagosomes containing rests of the biomaterial, along  
 378 with extracellular matrix mainly consisting of collagen fibres that were comparable to control tissues (Fig. 5). On  
 379 the other hand, animals grafted with MNPs showed very similar behaviour regardless of the specific group  
 380 considered (FAH-MNPs, FAH-MNPs-F and MNPs-INJ). In all these groups, we found numerous host cells  
 381 compatible with macrophages containing abundant intracellular MNPs that tended to keep their original

382 polycrystalline aggregate pattern inside the cells. Most of the particles gathered in cytoplasmic vesicles that could  
383 correspond to endosomes or secondary lysosomes, as well as large phagosomes. MagNP-OH were also found in  
384 the extracellular space. No signs of necrosis or cell alterations were detected in any of the study groups. These  
385 findings confirm the high biocompatibility of the different materials used in this study. In agreement with previous  
386 reports, our results suggest that iron oxide nanoparticles are mostly engulfed within the human cells and do not  
387 cause any detectable alterations in these cells [10, 50].

388  
389



390 **Figure 5. Representative images corresponding to the ultrastructural analysis of materials grafted *in vivo***  
391 **for 12 weeks.** CTR: control animals; FAH: fibrin-agarose hydrogels; FAH-MNPs: FAH containing MagNP-OH;  
392 MNPs-INJ: MNPs injected subcutaneously. Black arrow: phagosome containing agarose; white arrow: MNPs. The  
393 inserts images correspond to higher magnifications of the same images. Scale bars: 300  $\mu\text{m}$  (large images) and 20  
394  $\mu\text{m}$  (inserts).

395  
396

397 Once the local implant site was analysed, we evaluated the morphology, structure and function of several major  
398 distal organs of each animal to determine the possible distal effects of each biomaterial as part of the global  
399 biocompatibility and biosafety assessment required for future clinical use [45]. In this regard, the whole-body MRI  
400 scan analysis of each animal and the specific analysis of four key organs playing a role in metabolizing and  
401 processing a biomaterial grafted *in vivo* -liver, kidneys, lymph nodes and spleen- revealed a perfectly normal  
402 morphology devoid of detectable alterations (Supplementary Fig. 1). No MNPs were detected by MRI in any of  
403 these organs. Similarly, analysis of the different organs using magnetometry, revealed a negative signal in all  
404 animals after 12 weeks of *in vivo* follow-up. These results suggest that MagNP-OH stayed at the grafting site and  
405 did not tend to migrate, supporting the stability of this type of MNPs.

406 At the histological level, the structural analysis of distal organs confirmed the absence of alterations during the  
407 whole study. Indeed, no signs of inflammation, fibrosis, necrosis or other detectable tissue alterations were  
408 observed in histological sections of liver, kidneys, lymph nodes and spleen stained with H&E in any of the groups  
409 (Supplementary Fig. S2). Similarly, PAS staining analysis (Supplementary Fig. S3) confirmed that the content of

410 glycogen was normal in hepatocytes of all groups of animals, and the glomerular and non-glomerular basement  
411 membranes were also free from detectable alterations. These results are in agreement with previous studies  
412 demonstrating that this type of MNPs coated with different polymers can be safely used without significant  
413 histological alterations of vital organs [14, 51], whereas other types of particles were associated to histological  
414 lesions in liver and kidney [52].

415 To identify any possible particle migration to distal organs, we also analysed these organs using the Perls  
416 histochemical technique, which is specific for detection of iron in cells and tissues. Results showed very few or no  
417 particles in the liver and kidney at 1 and 12 weeks, but a positive reaction was found in spleen and lymph nodes at  
418 both analysed times (Fig. 6). These findings are in agreement with previous reports demonstrating that  
419 nanoparticles of different nature tend to be massively captured by cells of the mononuclear phagocyte system [49].  
420 Hence, we found that lymph nodes were Perls-negative in CTR and FAH group, whereas animals with grafted  
421 MNPs (FAH-MNPs, FAH-MNPs-F and MNPs-INJ) showed small Perls-positive areas after 1 week, and moderate  
422 to intense Perls-positive areas after 12 weeks, especially in the case of the injected MNPs. Then, we analysed both  
423 components of the rat spleen (the red and the white pulp), and we found that the staining area and intensity were  
424 higher in this organ than in the rest of organs. As expected, the red pulp of the spleen was very positive to the Perls  
425 method in all groups, including controls, but this reaction became significantly more intense after 12 weeks in  
426 FAH-MNPs, FAH-MNPs-F and MNPs-INJ groups ( $p < 0.05$ ). These findings are consistent with the primary  
427 function of the red pulp, which is related to filtering peripheral blood from antigens, foreign bodies and all kinds  
428 of substances that may arrive in the blood, blood iron turnover, as well as serving as a huge reservoir of monocytes  
429 [18]. The white pulp, however, was mostly negative for this staining technique, although the marginal zone (in  
430 which antigen-presenting cells, such as dendritic cells and macrophages exists) was positive at 12 weeks in FAH-  
431 MNPs, FAH-MNPs-F and MNPs-INJ groups. Quantification of the Perls-positive areas in the red pulp (Fig. 7)  
432 demonstrated no significant differences among samples at 1 week ( $p > 0.05$ ), but a significant increase was found  
433 at 12 weeks in the FAH-MNPs and MNPs-INJ groups ( $p < 0.05$ ). In fact, the three groups in which MNPs were  
434 grafted in animals, showed significant differences vs. control at week 12 ( $p < 0.05$ ). These results were  
435 corroborated at the ultrastructural level by TEM analysis confirming the presence of macrophages containing  
436 electron-dense iron-rich granular material identified as iron by EELS in all experimental groups (Fig. 7). In contrast  
437 with the macrophages observed within grafted biomaterials, in spleen, these cells contained iron-rich granular  
438 intracytoplasmic vesicles, but polycrystalline aggregates were not detected.

439 The presence of abundant cells containing iron in the spleen of all animal groups could be explained by the  
440 important role that the spleen plays in mechanical filtration of red blood cells and haemoglobin iron recycling and  
441 turnover [18]. The increase observed in animals in which MagNP-OH were grafted, strongly suggests that MNPs  
442 could progressively reach the spleen through blood circulation, as other authors demonstrated by intraperitoneal  
443 injection of RITC-labeled MNPs [10, 50]. The fact that our magnetometry and MRI analyses were negative could  
444 probably be explained by the low concentration of MagNP-OH that reached the spleen, which was probably below  
445 than 30  $\mu\text{g}$ , which is the minimum concentration required for detection by magnetometry and MRI. Another  
446 possibility is that MagNP-OH were progressively transformed into non-magnetic iron forms by host cells as  
447 previously suggested [47]. Interestingly, previous works showed that superparamagnetic iron-oxide NPs show  
448 identical distribution pattern when administered *in vivo* [51].

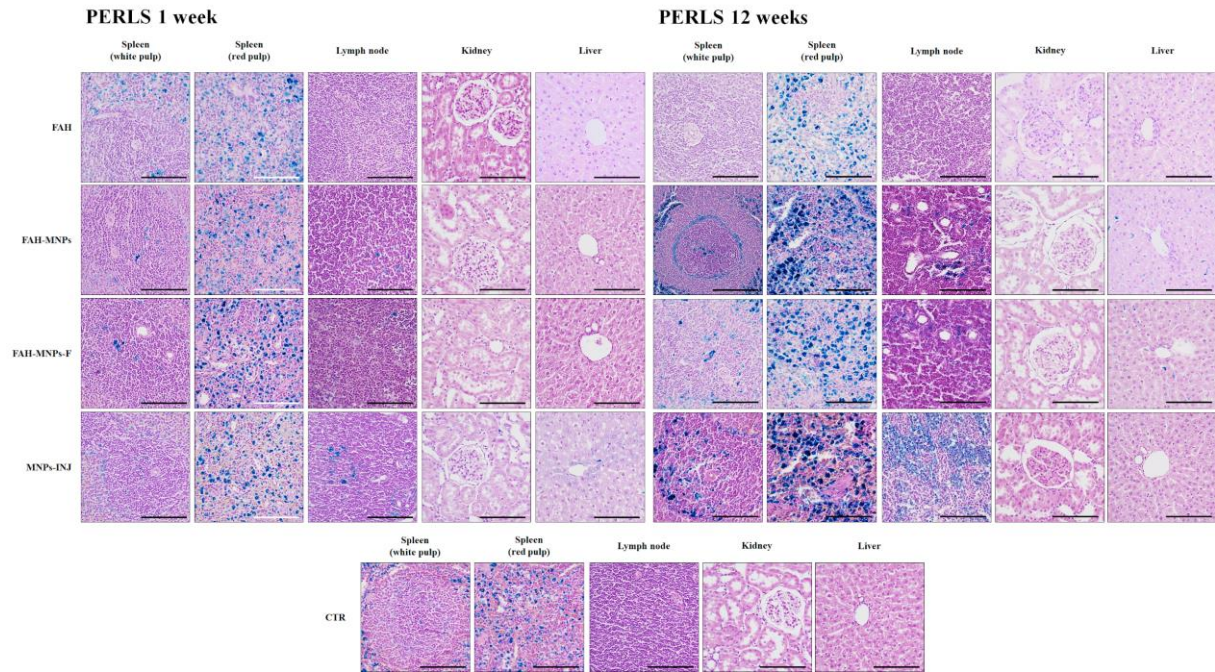
449 In consequence, our histological results, in line with results published by other authors, highlight the relevance of  
450 the administration route and NPs size in the subsequent organic biodistribution [10], and confirm that MagNP-OH

451 tend to remain stable at the implant site, with some particles biodistributed to lymphoid organs, without altering  
452 their histological structure and function.

453

454

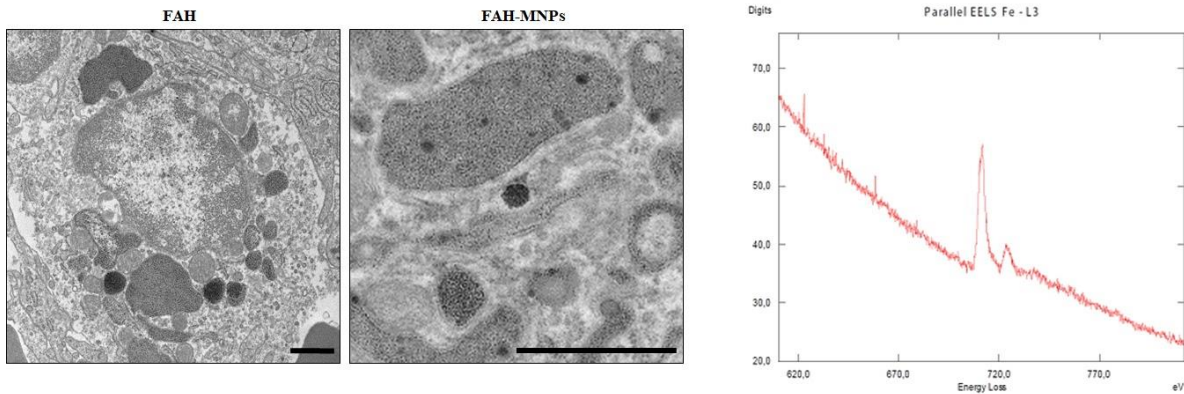
455



456 **Figure 6. Perl's histochemical results of distal organs at 1 and 12 weeks.** FAH: fibrin-agarose hydrogels; FAH-  
457 MNPs: FAH containing MagNP-OH; FAH-MNPs-F: FAH containing MagNP-OH subjected to magnetic field  
458 during gelation; MNPs-INJ: MNPs injected subcutaneously; CTR: control animals. Scale bar 100  $\mu$ m.



PERLS-POSITIVE AREAS IN SPLEEN RED PULP	CTR	FAH	FAH-MNPs	FAH-MNPs-F	MNPs-INJ
1 week	3.28 ± 0.55	3.54 ± 0.75 (p = 0.9990)	5.77 ± 0.61 (p = 0.4977)	9.64 ± 1.38 (p = 0.0818)	8.61 ± 0.72 (p = 0.1338)
12 weeks	7.77 ± 0.89	5.43 ± 0.15 (p = 0.5679)	22.84 ± 1.83 (p = 0.0056)*	18.62 ± 1.81 (p = 0.0370)*	28.25 ± 2.45 (p = 0.0004)*
1 week vs. 12 weeks	(p = 0.2134)	(p = 0.9990)	(p = 0.0010)*	(p = 0.1070)	(p = 0.0009)*



460 **Figure 7. Quantitative results of Perls positive histochemical reaction and EELS in the red pulp of the spleen**  
 461 **in each group and control.** The table on top shows the results of the quantification of the percentage of the area  
 462 corresponding to Perls-positive signal. The figures below show illustrative ultrastructural images of macrophages  
 463 containing iron in intracellular phagosomes corresponding to two groups of animals (FAH and FAH-MNPs), along  
 464 with an EELS spectrum with a peak corresponding to intracellular iron. CTR: control animals; FAH: fibrin-agarose  
 465 hydrogels; FAH-MNPs: FAH containing MagNP-OH; FAH-MNPs-F: FAH containing MagNP-OH subjected to  
 466 a magnetic field during gelation; MNPs-INJ: MNPs injected subcutaneously. Values in the table are shown as  
 467 mean ± standard deviation for each group of animals and each follow-up time, and the statistical p values  
 468 corresponding to the comparison of these values with CTR are shown in brackets. In the last row, the statistical p  
 469 values corresponding to the comparison of values at 1 week vs. values at 12 weeks are shown for each study group.  
 470 Significant differences ( $p < 0.05$ ) are highlighted with asterisks (\*). Scale bar for FAH = 1  $\mu\text{m}$  and scale bar for  
 471 FAH-MNPs = 2  $\mu\text{m}$ .

472

473

HAEMOGRAM									Weeks
General count					WBC/White cells				
WBC ( $10^3$ ) $\mu\text{L}^{-1}$	RBC ( $10^6$ ) $\mu\text{L}^{-1}$	HGB g/dL	HCT %	PLT ( $10^5$ ) $\mu\text{L}^{-1}$	LYM %	MXD %	NEUT %		
FAH	3.04 ± 1.51*	7.14 ± 0.22*	13.5 ± 0.52	39.54 ± 1.1	5.16 ± 1.99	45.68 ± 23.56	32.56 ± 22.96	21.76 ± 4.64	
	4.56 ± 3.31	7.61 ± 0.06	14.14 ± 0.51	42.28 ± 0.66	4.60 ± 2.59	64.38 ± 14.8	12.96 ± 0.86	22.66 ± 14.22	3
	2.75 ± 0.26*	8.04 ± 0.4	14.15 ± 0.27	43.78 ± 1.3	6.57 ± 0.23	77.63 ± 4.06	9.25 ± 3.02	13.13 ± 5.75	5
	9.74 ± 3.89	8.15 ± 0.38	14.32 ± 0.2	44.06 ± 1.93	5.11 ± 3.63	68.5 ± 16.18	9.32 ± 3.65	22.18 ± 13.58	12
FAH-MNPs	2.4 ± 1.27	7.47 ± 0.64	13.22 ± 1.48	40.02 ± 4.35	5.63 ± 2.96	42.08 ± 26.77	33.02 ± 25.75	24.84 ± 12.87	1
	5.18 ± 3.11	7.51 ± 0.3	14.16 ± 0.76	42.26 ± 2.17	3.82 ± 2.16	62.02 ± 15.52	13.34 ± 2.57	24.64 ± 16.25	3
	2.48 ± 1.09	8.11 ± 1.48*	14.18 ± 9.93	44.27 ± 1.72	6.24 ± 2.57	72.7 ± 16.81	5.92 ± 1.78	21.08 ± 9.9	5
	2.94 ± 3.52	7.83 ± 0.68	14.16 ± 0.76	42.48 ± 4.15	8.74 ± 0.84	80.32 ± 3.35*	15.28 ± 4.59	2.56 ± 5.96	12

FAH-MNPs-F	3.63 ± 2.1	7.76 ± 0.38	13.83 ± 0.25	42.43 ± 1.85	5.61 ± 1.21	66.25 ± 8.58	13.83 ± 5.93	19.93 ± 6.41	1
	2.46 ± 0.46	7.62 ± 0.44	13.58 ± 0.39	41.18 ± 1.69	6.31 ± 0.72	76.02 ± 3.35	11.04 ± 1.35	12.94 ± 2.11	3
	5.36 ± 4.05	7.77 ± 4.09*	13.91 ± 0.6	42.73 ± 1.81	3.62 ± 2.48	68 ± 12.91	16.02 ± 7.07	15.98 ± 6.97	5
	5.72 ± 1.73	8.46 ± 0.62*	14.52 ± 0.6	45.66 ± 3.1	3.78 ± 4.1	69 ± 13.41	12.64 ± 2.97	18.36 ± 11.6	12
MNPs-INJ	2.48 ± 0.43	7.82 ± 0.24	13.78 ± 0.42	42.8 ± 1.86	4.88 ± 2.75	72.08 ± 6.03	12.53 ± 1.24	15.4 ± 6.02	1
	1.92 ± 0.64	7.54 ± 0.26	13.5 ± 0.24	41.22 ± 1.51	6.26 ± 0.73	73.2 ± 7.71	14.92 ± 5.72	11.88 ± 2.58	3
	1.78 ± 0.29	8.03 ± 0.23 *	14.08 ± 0.83	43.94 ± 2	5.94 ± 2.82	74.5 ± 3.71	10.82 ± 4.98	14.68 ± 6.67	5
	7.1 ± 3.74	7.57 ± 0.89	13.75 ± 1.61	41.45 ± 5.4	4.33 ± 4.58	65.83 ± 4.67	10.03 ± 3.42	24.15 ± 6.5	12
CTR	5.93 ± 3.46	7.72 ± 0.11	13.9 ± 0.5	42.25 ± 1.07	2.58 ± 2.71	63.03 ± 15.39	14.33 ± 6.75	22.65 ± 13.16	

474

475 **Table 1. Haematological profile.** Summary of the mean and SD of parameters evaluated at 1, 3, 5 and 12 weeks.

476 White blood cells (WBC), erythrocytes count (RBC), concentration of haemoglobin (HGB), haematocrit count

477 (HCT), platelets (PLT), lymphocytes (LYM), monocytes-basophils-eosinophils (MXD), neutrophils (NEUT).

478 Significant differences ( $p < 0.05$ ) between experimental and control groups are highlighted with asterisks (\*).

479

480 After that the morphology and structure of local and distal tissues and organs were determined, we analysed the

481 effect of the different biomaterials on each animal group at the functional level. In this regard, haematological

482 studies revealed that all parameters evaluated here were within the physiological range of normal values described

483 in the literature for the Wistar rat (Table 1) [52]. However, some specific parameters showed significant differences

484 with the control animals used in this study. In the case of the red blood cells (RBC), we observed a significant

485 decrease of RBC counts in the FAH group at 1 week as compared to controls ( $p = 0.009$ ), which could be a

486 consequence of the recent surgical procedure. In contrast, a significant increase of the number of RBC was

487 observed after 5 weeks in FAH-MNPs ( $p = 0.016$ ), FAH-MNPs-F ( $p = 0.016$ ) and MNPs-INJ ( $p = 0.028$ ), and also

488 after 12 weeks for FAH-MNPs-F ( $p = 0.028$ ) as compared to controls. Interestingly, the increase of RBC values

489 was not accompanied by significant variations of the concentration of haemoglobin (HGB) or haematocrit (HCT).

490 The leukocyte count (WBC) showed a transient reduction in the FAH group at 5 weeks as compared to controls

491 ( $p = 0.009$ ), although the leukocyte formula was normal for all the study groups except for an increase of

492 lymphocytes (LYM) at 12 weeks in FAH-MNPs group ( $p = 0.010$ ). Finally, the evaluation of platelets (PLT)

493 showed an increase in all experimental groups over time as compared to control animals. All these variations,

494 which fell into the normal parameters of healthy Wistar rats [52], could be related to the host adaptive physiological

495 response to the surgical procedure, healing process, active hydrogel biodegradation and MagNP-OH phagocytosis

496 being these results in line with the histological findings. A similar result was found for the biochemical parameters

497 analysed in plasma of each animal, which were normal in most cases (Table 2). First, the levels of circulating iron

498 were similar to control animals at all study times ( $p > 0.05$ ). The lack of increase of circulating free iron supports

499 the idea that MNPs remained stable and were not able to release a significant amount of iron to the circulation.

500 Similarly, most hepatic function-related parameters fell within the physiological range of this species, except for

501 an initial transient decrease of ALT in MNPs-INJ ( $p = 0.028$ ) that normalized thereafter. Finally, the two

502 biochemical markers of renal function (urea and creatinine) were normal in all study groups. Additionally, the

503 renal function-related parameters urea and creatinine (CREJ2) showed a transitory increase over the time in all

504 experimental groups as compared to controls, which tended to normalize with time.

505 Altogether, these haematological and biochemical results confirmed that the use of MagNP-OH is safe and *in vivo*

506 implantation of these MNPs is not associated to a vital organ failure. Although some slight variations were found

507 in specific groups of animals, values were in agreement with the physiological ranges described in the literature

508 [52], and showed a clear normalization over time. In addition, the normalization of blood and biochemical  
 509 parameters is in line with the quantitative results observed in Wistar rats in which the sciatic nerve was repaired  
 510 with acellular nerve grafts [35]. These findings confirm again that both administration routes for the MagNP-OH  
 511 (injected or encapsulated) were safe for the host animal. In contrast, a previous study showed that the high-dose  
 512 oral administration of other types of nanoparticles based on silver was related to hepatic and renal affection at the  
 513 biochemical level, what clearly differed from our findings [52]. Finally, the haematological and biochemical  
 514 profiles were in concordance with the histological and MRI results showing normal structure and morphology of  
 515 distal organs. All this suggests that the *in vivo* injection and the subcutaneous implantation of the magnetic  
 516 materials generated in this work was fully biocompatible and fulfilled the strict biosafety criteria required for future  
 517 clinical use.  
 518

BIOCHEMICAL					
	Liver	Kidney	Other parameters		
	ALT	CREJ2	UREA	Fe	Weeks
	U/L	mg/dl	mg/dl	µg/dl	
FAH	46.28 ± 10.26	0.75 ± 0.08	42.32 ± 6.71	162.27 ± 0.29	1
	40.44 ± 7.38	0.65 ± 0.14	43.28 ± 7.34	170.25 ± 0.33	3
	41.35 ± 17.39	0.6 ± 0.24	38.08 ± 13.76	164.21 ± 0.61	5
	53.54 ± 16.03	0.6 ± 0.08	36.94 ± 2.65	181.19 ± 0.22	12
FAH-MNPs	141 ± 144.53	0.7 ± 0.15	46.66 ± 8.73	147.31 ± 0.31	1
	79.2 ± 65.15	0.72 ± 0.08	43.84 ± 5.97	187.51 ± 0.32	3
	42.08 ± 10.65	0.66 ± 0.15	38.22 ± 2.67	171.19 ± 0.40	5
FAH-MNPs-F	74.68 ± 60.94	0.54 ± 0.11	35.08 ± 4.48	249.36 ± 1.91	12
	45.75 ± 6.72	0.84 ± 0.18	37.5 ± 8.76	157.85 ± 0.42	1
	46.82 ± 11.49	0.69 ± 0.1	41.5 ± 4.6	160.15 ± 0.15	3
	46.61 ± 26.92	0.53 ± 0.05	39.59 ± 4.93	172.2 ± 0.27	5
MNPs-INJ	45.28 ± 9.17	0.66 ± 0.05	38.72 ± 5.84	148.91 ± 0.10	12
	30.2 ± 7.83*	0.65 ± 0.11	39.3 ± 7.57	155.15 ± 0.25	1
	35.94 ± 6.19	0.53 ± 0.08	38.98 ± 4.74	183.92 ± 0.22	3
	62.86 ± 30.07	0.71 ± 0.11	38.56 ± 4.89	168.49 ± 0.26	5
CTR	44.62 ± 10.09	0.74 ± 0.11	39.58 ± 5.2	164.91 ± 0.29	12
	39.55 ± 5.55	0.46 ± 0.14	34 ± 2.81	184.36 ± 0.23	

519  
 520 **Table 2. Biochemical profile.** Summary of the mean and SD of parameters evaluated at 1, 3, 5 and 12 weeks.  
 521 Alanine aminotransferase (ALT), urea (UREA), creatinine (CREJ2) and iron (Fe). Significant differences ( $p <$   
 522 0.05) between experimental and control groups are highlighted with asterisks (\*).  
 523

524 In summary, although the particles remained at the grafting site after 12 weeks, these results suggest that MagNP-  
 525 OH fulfil the biosafety and biocompatibility requirements for future clinical use. Incorporation of these MNPs in  
 526 fibrin-agarose biomaterials allows the generation of novel biomaterials with improved biomechanical properties  
 527 with guarantees of biosafety and biocompatibility demonstrated at the morphological, structural and functional  
 528 levels. As an alternative route of delivery, tissue-like biomaterials allow efficient control of the MNPs  
 529 biodistribution *in vivo*. Biodistribution analysis demonstrated that our strategy supports the local use of the  
 530 MagNP-OH, which were mostly confined to the implantation area. However, long-term studies are still needed to  
 531 determine the time required for the complete biodegradation and/or metabolization of the implanted MagNP-OH.  
 532 In addition, tissue-like biomaterials based on fibrin-agarose combined with MagNP-OH allows easy handling and  
 533 straightforward surgical implant of these nanoparticles, and facilitates local *in vivo* encapsulation of MagNP-OH  
 534 as compared to injected MagNP-OH. In addition, the methodology described in the present manuscript also

535 allowed the generation of novel biomaterials with a definite structural alignment using magnetic fields during the  
536 gelation of the biomaterial. This could be advantageous for reproduction and treatment of human tissues requiring  
537 a specific 3D structural organization such as the human cornea [53], tendon [54] and cartilage [55] and also other  
538 tissues with an anisotropic behaviour such as the human skin, nerve and oral mucosa and palate [56]. However,  
539 future clinical trials should demonstrate the usefulness of these tissue-like products.

540

#### 541 **4. Conflicts of interest**

542 The authors declare that they have no known competing financial interests or personal relationships that could  
543 have appeared to influence the work reported in this paper.

544

#### 545 **5. Author contributions**

546 MTLL performed magnetic particles characterization. IAR and MA developed in vitro analyses of  
547 biocompatibility. ABBE, JDGD and MTLL performed the mechanical properties. FC, IAR, ABBE and VC  
548 performed the surgery of animals. FC, IAR and VC performed and analysed the magnetic resonance imaging. IAR,  
549 ABBE and VC developed and analysed the data of haematological and biochemical studies. FC, IAR, ABBE and  
550 VC developed histological and histochemical studies. IAR and VC analysed data of histology. RC, IAR and VC  
551 performed the ultrastructural study. MTLL, ABBE and PK, performed magnetometry. FC and MA statistical  
552 analyses. IAR, FC, VC, MA and MTLL performed the experimental design and wrote this work.

553

#### 554 **6. Acknowledgements**

555 This study was supported by the following grants:

- 556 • Grants FIS-PI17/0391 and FIS-PI17/0393 from Instituto de Salud Carlos III - ISCIII (Plan Nacional de  
557 Investigación Científica, Desarrollo e Innovación Tecnológica I+D+i from the Spanish Ministerio de Ciencia  
558 e Innovación), co-financed by ERDF-FEDER, European Union.
- 559 • Award number AC17/00013 (NanoGSKin) by ISCIII thorough AES 2017 and within the EuroNanoMed  
560 framework.
- 561 • Grant FIS2017-85954-R funded by Ministerio de Economía, Industria y Competitividad, MINECO, and  
562 Agencia Estatal de Investigación, AEI, Spain, cofunded by Fondo Europeo de Desarrollo Regional, FEDER,  
563 European Union.
- 564 • Grants CS PI-0257-2017 and CSyF PE-0395-2019 from Consejería de Salud y Familias, Junta de Andalucía,  
565 Spain.
- 566 • Grant nº Res SECYT 411/18 from SECYT (Secretary of Science and Technology of National University of  
567 Córdoba, Argentina)
- 568 • Project Future Investments UCA JEDI, No. ANR-15-IDEX-01, project “RheoGel” by the French “Agence  
569 Nationale de la Recherche”.

570

571 Authors are grateful to Dr. Ariane Ruyffelaert for her proofreading service and for the technical assistance of  
572 Amalia de la Rosa Romero and Concepción López Rodríguez (Experimental Unit of the University Hospital  
573 Virgen de las Nieves, Granada, Spain).

574

575

576

577

578 **References**

579

- 580 [1] A. Cervadoro, C. Giverso, R. Pande, S. Sarangi, L. Preziosi, J. Wosik, A. Brazdeikis, P.  
581 Decuzzi, *PLoS One*, 8 (2013) e57332.
- 582 [2] K. Andreas, R. Georgieva, M. Ladwig, S. Mueller, M. Notter, M. Sittinger, J. Ringe,  
583 *Biomaterials*, 33 (2012) 4515-4525.
- 584 [3] X.W. Chen, Q.X. Mao, J.W. Liu, J.H. Wang, *Talanta*, 100 (2012) 107-112.
- 585 [4] J. Qin, K. Li, C. Peng, X. Li, J. Lin, K. Ye, X. Yang, Q. Xie, Z. Shen, Y. Jin, M. Jiang, G.  
586 Zhang, X. Lu, *Biomaterials*, 34 (2013) 4914-4925.
- 587 [5] S. Jiang, A.A. Eltoukhy, K.T. Love, R. Langer, D.G. Anderson, *Nano Lett*, 13 (2013)  
588 1059-1064.
- 589 [6] G.Y. Lee, W.P. Qian, L. Wang, Y.A. Wang, C.A. Staley, M. Satpathy, S. Nie, H. Mao, L.  
590 Yang, *ACS Nano*, 7 (2013) 2078-2089.
- 591 [7] M.J. Alonso, S. Cohen, T.G. Park, R.K. Gupta, G.R. Siber, R. Langer, *Pharm Res*, 10  
592 (1993) 945-953.
- 593 [8] S. Behrens, *Nanoscale*, 3 (2011) 877-892.
- 594 [9] K. Niemirowicz, K.H. Markiewicz, A.Z. Wilczewska, H. Car, *Adv Med Sci*, 57 (2012)  
595 196-207.
- 596 [10] L.H. Reddy, J.L. Arias, J. Nicolas, P. Couvreur, *Chem Rev*, 112 (2012) 5818-5878.
- 597 [11] C. Chouly, D. Pouliquen, I. Lucet, J.J. Jeune, P. Jallet, *J Microencapsul*, 13 (1996) 245-  
598 255.
- 599 [12] R. De Santis, A. Russo, A. Gloria, U. D'Amora, T. Russo, S. Panseri, M. Sandri, A.  
600 Tampieri, M. Marcacci, V.A. Dediu, C.J. Wilde, L. Ambrosio, *J Biomed Nanotechnol*, 11  
601 (2015) 1236-1246.
- 602 [13] M.T. Lopez-Lopez, G. Scionti, A.C. Oliveira, J.D. Duran, A. Campos, M. Alaminos, I.A.  
603 Rodriguez, *PLoS One*, 10 (2015) e0133878.
- 604 [14] L. Rodriguez-Arco, I.A. Rodriguez, V. Carriel, A.B. Bonhome-Espinosa, F. Campos, P.  
605 Kuzhir, J.D. Duran, M.T. Lopez-Lopez, *Nanoscale*, 8 (2016) 8138-8150.
- 606 [15] X.B. Zeng, H. Hu, L.Q. Xie, F. Lan, W. Jiang, Y. Wu, Z.W. Gu, *Int J Nanomedicine*, 7  
607 (2012) 3365-3378.
- 608 [16] N. Bock, A. Riminucci, C. Dionigi, A. Russo, A. Tampieri, E. Landi, V.A. Goranov, M.  
609 Marcacci, V. Dediu, *Acta Biomater*, 6 (2010) 786-796.
- 610 [17] A.B. Bonhome-Espinosa, F. Campos, I.A. Rodriguez, V. Carriel, J.A. Marins, A.  
611 Zubarev, J.D.G. Duran, M.T. Lopez-Lopez, *Soft Matter*, 13 (2017) 2928-2941.
- 612 [18] J.S. Kim, T.J. Yoon, K.N. Yu, B.G. Kim, S.J. Park, H.W. Kim, K.H. Lee, S.B. Park, J.K.  
613 Lee, M.H. Cho, *Toxicol Sci*, 89 (2006) 338-347.
- 614 [19] M. Alaminos, M. Del Carmen Sanchez-Quevedo, J.I. Munoz-Avila, D. Serrano, S.  
615 Medialdea, I. Carreras, A. Campos, *Invest Ophthalmol Vis Sci*, 47 (2006) 3311-3317.
- 616 [20] F. Campos, A.B. Bonhome-Espinosa, G. Vizcaino, I.A. Rodriguez, D. Duran-Herrera,  
617 M.T. Lopez-Lopez, I. Sanchez-Montesinos, M. Alaminos, M.C. Sanchez-Quevedo, V.  
618 Carriel, *Biomed Mater*, 13 (2018) 025021.
- 619 [21] V. Carriel, I. Garzon, J.M. Jimenez, A.C. Oliveira, S. Arias-Santiago, A. Campos, M.C.  
620 Sanchez-Quevedo, M. Alaminos, *Cells Tissues Organs*, 196 (2012) 1-12.
- 621 [22] V. Carriel, G. Scionti, F. Campos, O. Roda, B. Castro, M. Cornelissen, I. Garzon, M.  
622 Alaminos, *J Tissue Eng Regen Med*, 11 (2017) 1412-1426.
- 623 [23] V. Carriel, G. Vizcaino-Lopez, J. Chato-Astrain, D. Durand-Herrera, M. Alaminos, A.  
624 Campos, I. Sanchez-Montesinos, F. Campos, *Exp Eye Res*, 186 (2019) 107717.

625 [24] J. Chato-Astrain, F. Campos, O. Roda, E. Miralles, D. Durand-Herrera, J.A. Saez-  
626 Moreno, S. Garcia-Garcia, M. Alaminos, A. Campos, V. Carriel, *Front Cell Neurosci*, 12  
627 (2018) 501.

628 [25] I.A. Rodriguez, M.T. Lopez-Lopez, A.C. Oliveira, M.C. Sanchez-Quevedo, A. Campos,  
629 M. Alaminos, J.D. Duran, *J Tissue Eng Regen Med*, 6 (2012) 636-644.

630 [26] M.C. Sanchez-Quevedo, M. Alaminos, L.M. Capitan, G. Moreu, I. Garzon, P.V. Crespo,  
631 A. Campos, *Histol Histopathol*, 22 (2007) 631-640.

632 [27] M. Lopez-Lopez, I. Rodriguez, L. Rodriguez-Arco, V. Carriel, A. Bonhome-Espinosa, F.  
633 Campos, A. Zubarev, J. Duran, *Journal of Magnetism and Magnetic Materials*, 431 (2017)  
634 110-114.

635 [28] F. Campos, A.B. Bonhome-Espinosa, L. Garcia-Martinez, J.D. Duran, M.T. Lopez-  
636 Lopez, M. Alaminos, M.C. Sanchez-Quevedo, V. Carriel, *Biomed Mater*, 11 (2016) 055004.

637 [29] M.A. Rodriguez, M.T. Lopez-Lopez, J.D. Duran, M. Alaminos, A. Campos, I.A.  
638 Rodriguez, *Cryobiology*, 67 (2013) 355-362.

639 [30] V. Carriel, I. Garzon, M. Alaminos, M. Cornelissen, *Neural Regen Res*, 9 (2014) 1657-  
640 1660.

641 [31] Y. Li, H. Meng, Y. Liu, B.P. Lee, *ScientificWorldJournal*, 2015 (2015) 685690.

642 [32] S. Vieira, A. Morais, J. Silva-Correia, J. Oliveira, R.L. Reis, *Natural-Based Hydrogels:*  
643 *From Processing to Applications*, 2017.

644 [33] L. Gasperini, J.F. Mano, R.L. Reis, *J R Soc Interface*, 11 (2014) 20140817.

645 [34] F. Campos, A.B. Bonhome-Espinosa, J. Chato-Astrain, D. Sanchez-Porras, O.D. Garcia-  
646 Garcia, R. Carmona, M.T. Lopez-Lopez, M. Alaminos, V. Carriel, I.A. Rodriguez, *Front*  
647 *Bioeng Biotechnol*, 8 (2020) 596.

648 [35] J. Chato-Astrain, C. Philips, F. Campos, D. Durand-Herrera, O.D. Garcia-Garcia, A.  
649 Roosens, M. Alaminos, A. Campos, V. Carriel, *J Tissue Eng Regen Med*, 14 (2020) 789-806.

650 [36] V. Carriel, J. Garrido-Gomez, P. Hernandez-Cortes, I. Garzon, S. Garcia-Garcia, J.A.  
651 Saez-Moreno, M. Del Carmen Sanchez-Quevedo, A. Campos, M. Alaminos, *J Neural Eng*, 10  
652 (2013) 026022.

653 [37] A. Gloria, T. Russo, U. D'Amora, S. Zeppetelli, T. D'Alessandro, M. Sandri, M.  
654 Banobre-Lopez, Y. Pineiro-Redondo, M. Uhlarz, A. Tampieri, J. Rivas, T. Herrmannsdorfer,  
655 V.A. Dediu, L. Ambrosio, R. De Santis, *J R Soc Interface*, 10 (2013) 20120833.

656 [38] A.K. Gupta, M. Gupta, *Biomaterials*, 26 (2005) 3995-4021.

657 [39] M.T. Lopez-Lopez, A. Gomez-Ramirez, L. Rodriguez-Arco, J.D. Duran, L. Iskakova, A.  
658 Zubarev, *Langmuir*, 28 (2012) 6232-6245.

659 [40] A. Tampieri, T. D'Alessandro, M. Sandri, S. Sprio, E. Landi, L. Bertinetti, S. Panseri, G.  
660 Pepponi, J. Goettlicher, M. Banobre-Lopez, J. Rivas, *Acta Biomater*, 8 (2012) 843-851.

661 [41] A. Tampieri, E. Landi, F. Valentini, M. Sandri, T. D'Alessandro, V. Dediu, M. Marcacci,  
662 *Nanotechnology*, 22 (2011) 015104.

663 [42] J. Li, Z. Yuan, H. Liu, J. Feng, Z. Chen, *J Nanobiotechnology*, 17 (2019) 124.

664 [43] R. Weissleder, D.D. Stark, B.L. Engelstad, B.R. Bacon, C.C. Compton, D.L. White, P.  
665 Jacobs, J. Lewis, *AJR Am J Roentgenol*, 152 (1989) 167-173.

666 [44] C. Song, X. Meng, Y. Liu, A. Shen, C. Shao, K. Wang, H. Cheng, X. Fang, P. Wang, W.  
667 Bu, *Biomaterials*, 230 (2020) 119631.

668 [45] L. Rico-Sanchez, I. Garzon, M. Gonzalez-Andrades, A. Ruiz-Garcia, M. Punzano, A.  
669 Lizana-Moreno, J.I. Munoz-Avila, M.D.C. Sanchez-Quevedo, J. Martinez-Atienza, L. Lopez-  
670 Navas, R. Sanchez-Pernaute, R.I. Oruezabal, S. Medialdea, M.D.C. Gonzalez-Gallardo, G.  
671 Carmona, S. Sanbonmatsu-Gamez, M. Perez, P. Jimenez, N. Cuende, A. Campos, M.  
672 Alaminos, *J Tissue Eng Regen Med*, 13 (2019) 2142-2154.

673 [46] E.A. Neuwelt, C.G. Varallyay, S. Manninger, D. Solymosi, M. Haluska, M.A. Hunt, G.  
674 Nesbit, A. Stevens, M. Jerosch-Herold, P.M. Jacobs, J.M. Hoffman, *Neurosurgery*, 60 (2007)  
675 601-611; discussion 611-602.

676 [47] M. Wankhede, A. Bouras, M. Kaluzova, C.G. Hadjipanayis, *Expert Rev Clin Pharmacol*,  
677 5 (2012) 173-186.

678 [48] P. Lakhani, K.K. Dwivedi, N. Kumar, *J Mech Behav Biomed Mater*, 104 (2020) 103693.

679 [49] C. Gila-Vilchez, M.C. Manas-Torres, R. Contreras-Montoya, M. Alaminos, J.D.G.  
680 Duran, L.A. de Cienfuegos, M.T. Lopez-Lopez, *Philos Trans A Math Phys Eng Sci*, 377  
681 (2019) 20180217.

682 [50] E. Teeman, C. Shasha, J.E. Evans, K.M. Krishnan, *Nanoscale*, 11 (2019) 7771-7780.

683 [51] A.S. Zhang, C.A. Enns, *Hematology Am Soc Hematol Educ Program*, (2009) 207-214.

684 [52] N. Dasgupta, S. Ranjan, C. Ramalingam, M. Gandhi, *3 Biotech*, 9 (2019) 125.

685 [53] A. Isaacson, S. Swioklo, C.J. Cannon, *Exp Eye Res*, 173 (2018) 188-193.

686 [54] A. Sensini, C. Gualandi, A. Zucchelli, L.A. Boyle, A.P. Kao, G.C. Reilly, G. Tozzi, L.  
687 Cristofolini, M.L. Focarete, *Sci Rep*, 8 (2018) 17167.

688 [55] J.P. Wu, T.B. Kirk, M.H. Zheng, *J Orthop Surg Res*, 3 (2008) 29.

689 [56] P. Liu, J.Y. Zhu, B. Tang, Z.C. Hu, *J Microsc*, 270 (2018) 170-175.

690

691

692

693

694

695

696

697

698

699

700

701

702

703

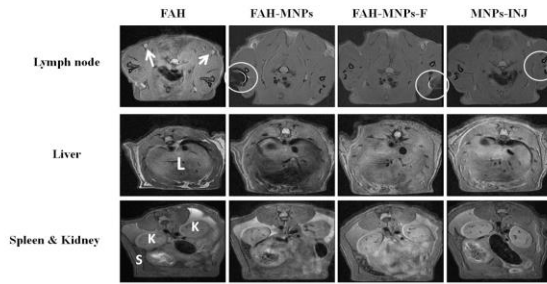
704

705

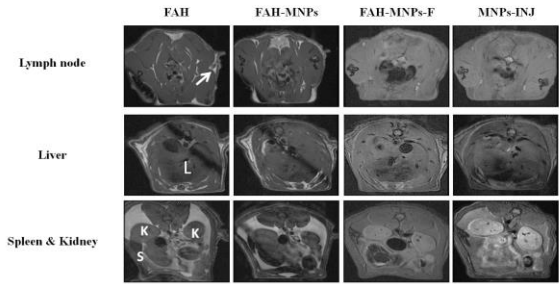
706

707

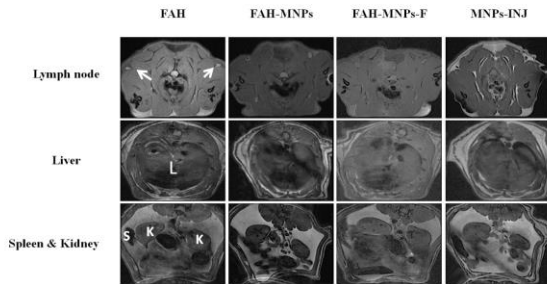
VITAL ORGANS 1 week



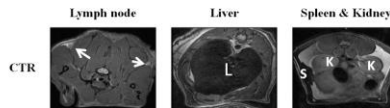
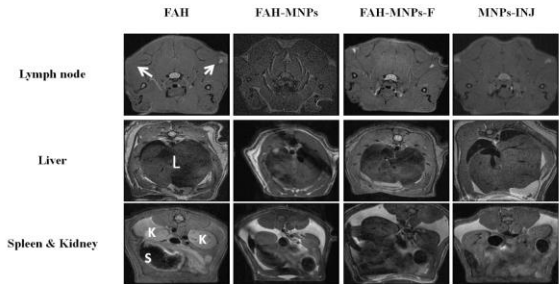
VITAL ORGANS 3 weeks



VITAL ORGANS 5 weeks



VITAL ORGANS 12 weeks



708

**Supplementary Figure S1. MRI analysis of vital organs at each study time.** FAH: fibrin-agarose hydrogels;

709

FAH-MNPs: FAH containing MagNP-OH; FAH-MNPs-F: FAH containing MagNP-OH subjected to a magnetic

710

field during gelation; MNPs-INJ: MNPs injected subcutaneously; CTR: control animals. White arrows: Lymph

711

node; L: Liver; S: Spleen; K: Kidney.

712

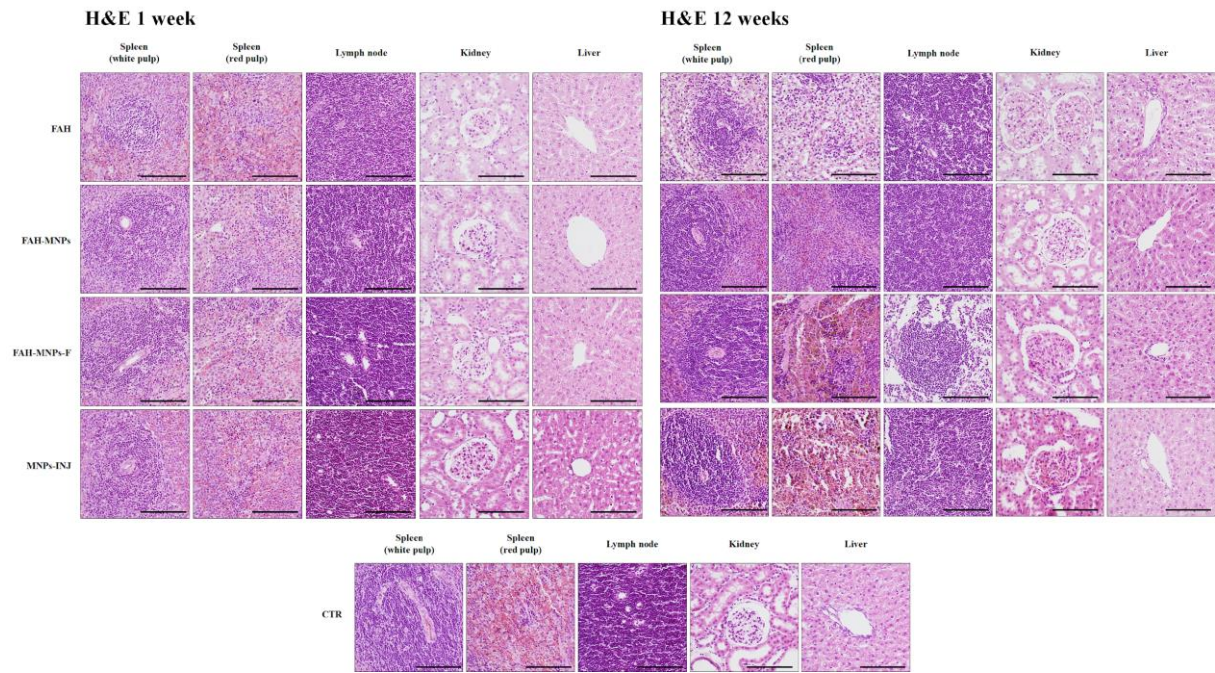
713

714

715

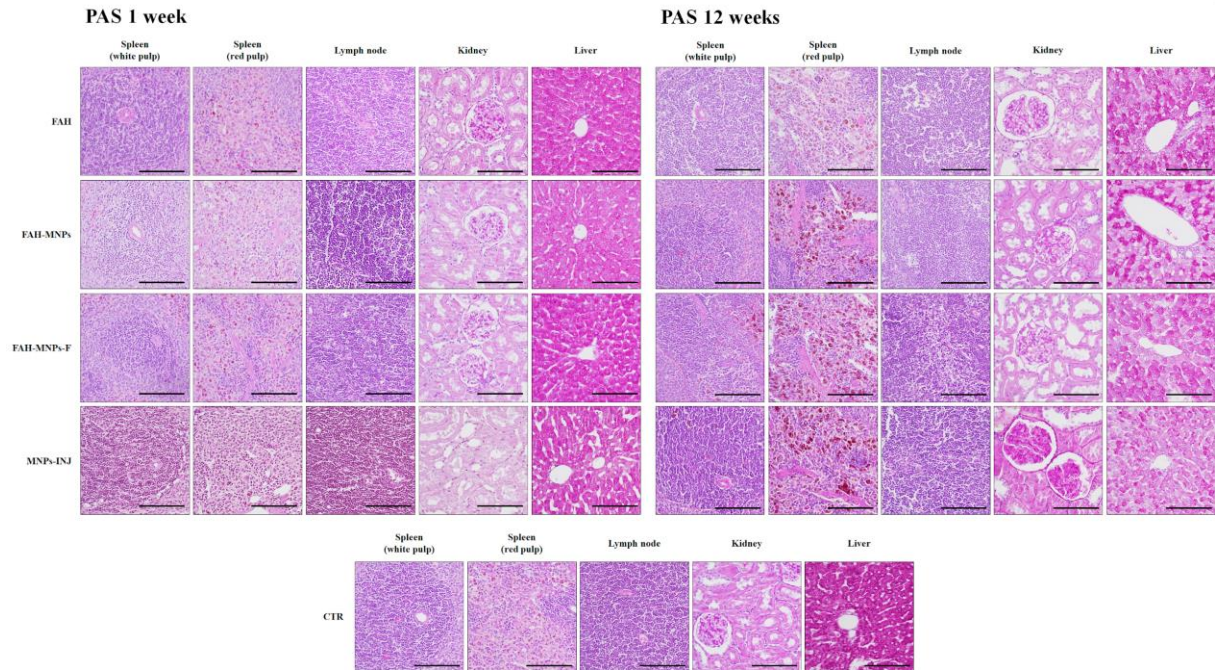


716



717 **Supplementary Figure S2. Histological analysis of four major distal organs using haematoxylin and eosin**  
718 **staining (H&E).** FAH: fibrin-agarose hydrogels; FAH-MNPs: FAH containing MagNP-OH; FAH-MNPs-F: FAH  
719 containing MagNP-OH subjected to a magnetic field during gelation; MNPs-INJ: MNPs injected subcutaneously;  
720 CTR: control animals. Scale bar 100  $\mu$ m.

721  
722  
723  
724  
725  
726  
727



728 **Supplementary Figure S3. Histochemical analysis of four major distal organs using the PAS method.** FAH:  
729 fibrin-agarose hydrogels; FAH-MNPs: FAH containing MagNP-OH; FAH-MNPs-F: FAH containing MagNP-OH  
730 subjected to magnetic field during gelation; MNPs-INJ: MNPs injected subcutaneously; CTR: control animals.  
731 Scale bar 100  $\mu$ m.  
732